The Astrophysical Journal Supplement Series, 193:1 (11pp), 2011 March doi:10.1088/0067-0049/193/1/1

AN EMPIRICAL *UBV RI JHK* COLOR–TEMPERATURE CALIBRATION FOR STARS

Guy Worthey[1] and Hyun-chul Lee[2]
[1] Department of Physics and Astronomy, Washington State University, Pullman, WA 99164-2814, USA
[2] Department of Physics and Geology, The University of Texas–Pan American, Edinburg, TX 78539-2999, USA
Received 2010 May 12; accepted 2010 September 21; published 2011 January 18

ABSTRACT

A collection of Johnson/Cousins photometry for stars with known [Fe/H] is used to generate color–color relations that include the abundance dependence. Literature temperature and bolometric correction (BC) dependences are attached to the color relations. The *JHK* colors are transformed to the Bessell & Brett homogenized system. The main result of this work is the tabulation of seven colors and the *V*-band BC as a function of $T_{\rm eff}$, log *g*, and [Fe/H] for $-1.06 < V - K < 10.2$ and an accompanying interpolation program. Improvements to the present calibration would involve filling photometry gaps, obtaining more accurate and on-system photometry, knowing better log *g* and [Fe/H] values, improving the statistics for data-impoverished groups of stars such as metal-poor K dwarfs, applying small tweaks in the processing pipeline, and obtaining better empirical temperature and BC relations, especially for supergiants and M stars. A way to estimate dust extinction from M dwarf colors is pointed out.

Key words: stars: abundances – stars: fundamental parameters – stars: general

Online-only material: machine-readable table

1. INTRODUCTION

Stellar evolutionary tracks and isochrones calculate physical radius, luminosity, and effective temperature. In order to compare with observable quantities, almost always magnitudes and colors, a transformation is essential. The need for such transformations is also felt when integrated light models (population synthesis models) are constructed for comparisons to colors from galaxies and star clusters. Color–temperature transformations are also used in spectral abundance analysis, design of observing strategies, computation of selection effects, and a host of incidental astronomical problems.

One way to approach this problem is to calculate line-blanketed synthetic spectra and integrate under filter transmission functions to get fluxes, which are then zeroed by comparison with Vega or other standard (Buser & Kurucz 1992; Bell & Gustafsson 1989). This is a convenient approach, but vulnerable to errors in all of the steps of the process: incorrect atmosphere structures, incorrect or incomplete line lists, incorrect treatment of convection, turbulence, non-LTE effects, or line broadening, incorrect filter transmissions, inaccurate spectrophotometry of the comparison star or stars, and finally, the photometry of the comparison star itself. Examples of suspicious circumstances include the fact that the blue edge of the *U* filter is set by Earth's atmosphere and will inevitably change with time and place, the fact that half the lines in the solar spectrum have yet to be identified (Kurucz 1992), and the fact that the absolute flux calibration for stars is uncertain by about 5% (e.g., Berriman et al. 1992). Recent examples of synthetic calibrations are VandenBerg & Clem (2003), Vazdekis et al. (1996), Lejeune et al. (1998), and Houdashelt et al. (2000).

There is need for empirical alternatives in the literature, and the present paper attempts to fill in that gap somewhat. The inspiration for this work comes from Green (1988). Green describes a global color–$T_{\rm eff}$ calibration generated for attachment to the Revised Yale Isochrones (Green et al. 1987) that provides colors tabulated for a (long) list of temperatures, surface gravities, and [Fe/H] values. The strategy used by Green was to begin with empirical color–color relations for solar-metallicity stars and adopt the ridge line as the starting place. Then one attaches a color–$T_{\rm eff}$ relation and adds [Fe/H] and gravity dependence by working differentially within synthetic color tables. The approach here is similar, but stays in the empirical regime longer in that the gravity and abundance dependences are fit to the stars themselves rather than via synthetic photometry. In a second phase, $T_{\rm eff}$ and the bolometric corrections (BCs) are attached to the fitted multidimensional space of $V-K$ color, gravity, and abundance. Synthetic colors are used at very low weight to guide the fits where there are few or no stars in the sample, but seemed to be superfluous except for metal-poor M giants, which do not exist in nature. Only oxygen-rich stars are considered here. Color–temperature relations for carbon-rich giants are given in Bergeat et al. (2001).

This paper is divided into sections on procedure, literature comparisons, and a concluding section. Supporting material (color–temperature table and interpolation program) is available at http://astro.wsu.edu/models/.

2. PROCEDURE

2.1. Stellar Data

The nucleus of the photometry catalog is the compilation of Morel & Magnenat (1978), which is firmly Johnson system. Many other photometry sources were included. These include Veeder (1974), Bessell (1991), Stetson (1981), da Costa & Armandroff (1990), Wood et al. (1983), Wood & Bessell (1983), von Braun et al. (1998), Carney (1983), Cohen et al. (1978, 1980), Elias et al. (1982, 1985), Frogel et al. (1978, 1979, 1981, 1983, 1990), Persson et al. (1980), da Costa et al. (1981), Cohen & Frogel (1982), Leggett et al. (2001), Dahn et al. (2002), and the Two Micron All Sky Survey (2MASS) point-source catalog.

As a first try at assigning abundance measurements to the list of 4496 stars, the Cayrel de Strobel et al. (2001), McWilliam (1990), and Edvardsson et al. (1993) abundance catalogs were consulted. M giants with good photometry were artificially assigned an [Fe/H] of zero except those that belong to clusters, in which case the cluster metallicity was adopted. M dwarfs were assigned an [Fe/H] based on their kinematics, most of which

came from Veeder (1974). Young disk objects were assigned [Fe/H] = −0.1, old disk −0.5, and halo −1.5. Cluster stars naturally inherited the cluster metallicity. Cluster abundances came from mostly secondhand compilations (Worthey et al. 1994; von Braun et al. 1998; Frogel et al. 1978). An abundance of +0.3 was adopted for NGC 6791 (Worthey & Jowett 2003). LMC field stars were assigned −0.3 and stars in the Small Magellanic Cloud (SMC) −0.6. Some supergiants and very hot stars were artificially assigned [Fe/H] = 0 when no abundance was available, but many had literature abundances. Unfortunately, a complete citing of the abundance sources cannot be given, as notes on some of the (perhaps 5%) abundance assignments have been lost. A total of 2090 usable stars had abundances, although the number is considerably less for any given photometric color. Odd holes appear in the final data set. For instance, a primary source for M dwarf colors is Veeder (1974) from which *J*-band data are missing. *U*-band data are hard to find for cool stars. Available *R*-band data have gaps as well. To try to fill in the "K dwarf desert" (see below) we also scoured Gray et al. (2003, 2006) and Casagrande et al. (2006) for photometry and abundance information.

Solar metallicity mean relations for all spectral types from Johnson (1966) and Bessell & Brett (1988) were included in the list, with [Fe/H] = −0.1 assumed for these "stars."

2.2. Photometric Systems

All, we think, would agree that the collection of the various photometric systems are, collectively, an admirable effort but also a bit of a mess due to the fact that one telescope/site/detector combination is a unique thing, not transferable to other telescopes in other places with different equipment. This is mostly overcome by observing standard stars that have been observed many times by one setup and should therefore be internally homogeneous: a photometric "system." The Morel & Magnenat (1978) catalog is on the "Johnson" photometric system. For colors involving *RI*, the target system was "Cousins" and we applied the transformation equations of Bessell (1979, 1983) to transform the Johnson data except for *R*−*I*, for which we used a tracing of Figure 3 from Bessell (1983) rather than the formula given in the paper. Additional optical data that were already on the Cousins system were left there.

Infrared data was imported from five different systems (and this is mild compared to the number of systems that have proliferated over the years). As a target system, we chose the homogenized system of Bessell & Brett (1988). Transformations from Johnson system, CIT system, and AAO system were used as provided in Bessell & Brett (1988). Some 2MASS data, mostly attached to NGC 6791 stars in the present stellar catalog, were transformed via Carpenter (2001) formulae to the Bessell & Brett (1988) system.

Corrections for interstellar extinction were done using the Cardelli et al. (1989) extinction curve. Note that corrections are applied differently for Johnson *RI* than for Cousins *RI* since the filters are at substantially different wavelengths. Such wavelength differences cause negligible correction differences at infrared wavelengths.

2.3. Color–Color Fitting

The photometrically homogenized, dereddened stellar data were then presented to a series of additional processing steps. A multivariate polynomial fitting program (a modification of the one used in Worthey et al. 1994 to fit spectral indices as a function of stellar atmosphere parameters) was applied to the data. The dependent variable chosen was *V*−*K* because it is monotonically increasing with temperature and insensitive to abundance. *V*−*K* is a fabulous temperature indicator in stars cooler than the Sun, and, because of its monotonicity, can still serve as a temperature-like variable for hotter stars. Terms of up to order $(V-K)^6$ could be included, and up to quadratic terms of log *g*, [Fe/H], and cross-terms. Chemically peculiar stars such as carbon stars were excluded from the fit.

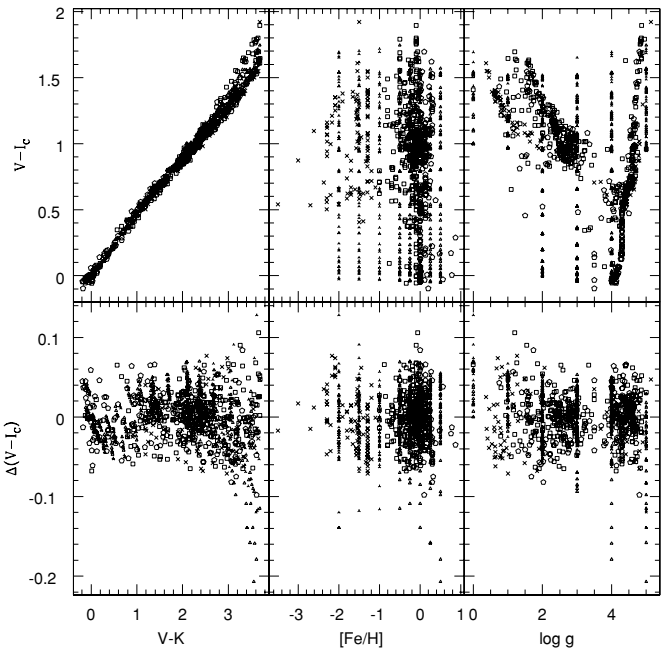

Figure 1. Illustration of the fitting process in the warm temperature range, using the *V*−*I* color. Smaller-size three-vertex symbols are synthetic photometric points that were not allowed to affect the fit if real stars were present, open for metal-rich "stars" and skeletal for metal-poor "stars." Open pentagons are metal-rich stars, open squares are between [Fe/H] = −1 and 0, and skeletal squares are metal-poor. These choices can be directly seen in the two, middle [Fe/H] panels. The top row of panels is *V*−*I* vs. *V*−*K*, [Fe/H], and log *g*, and the bottom row of panels is the data minus fit residuals vs. the same three variables. These plots vaguely mimic what the fitting program shows as it operates, although the fitting program can better isolate and display arbitrarily defined stellar groups, and also shows fits.

The color range was divided into five widely overlapping sections and each range was independently fit. For example, the second-hottest temperature section, for the color *V*−*I*, is displayed in Figure 1. The specific polynomial terms allowed in the fit could be different for each temperature section. This allowed, for instance, [Fe/H] sensitivity to be manually phased out if desired. The fits were done many times. Outlier data points were rejected manually with the aid of a graphical interface that allowed the name and parameters of each star to be scrutinized before rejection. Before one (of seven) color fits in one (of five) temperature regimes passed inspection, it was examined, both raw and as residuals from the fit, against all three variables of color, gravity, and abundance. Data rejection and polynomial term additions and subtractions were done iteratively with the aid of *f*-test statistics. In an approximation of what appears during the fitting process, Figure 1 shows both raw data and residuals after the fit as a function of *V*−*K* color, [Fe/H], and log *g*, with symbol types varying as a function of abundance. Synthetic color points are also shown, for purposes of illustration, although we emphasize that the synthetic colors

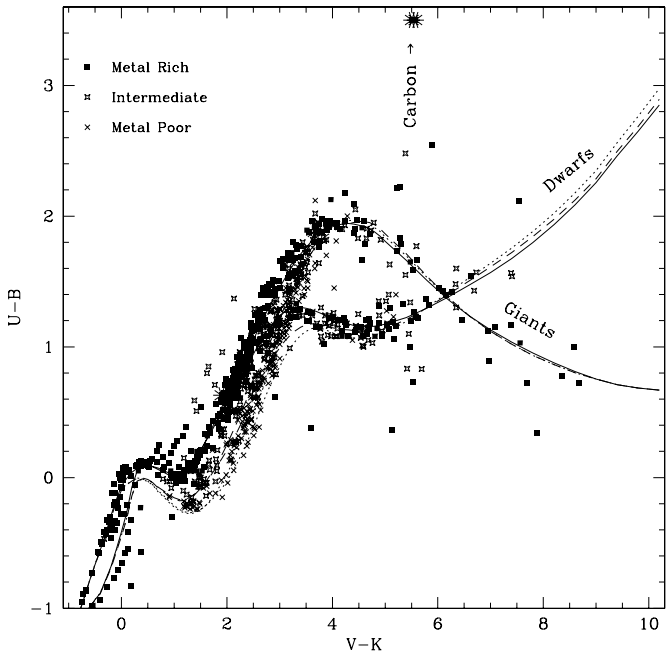

Figure 2. $U-B, V-K$ color–color diagram for unculled stars. Stars have different symbol types for metal-rich ([Fe/H] > -0.2), metal-poor ([Fe/H] < -1.2), and intermediate abundance ranges. Calibrations for typical giant and typical dwarf gravities are drawn in solid for [Fe/H] $= 0$, dashed for [Fe/H] $= -1$, and dotted for [Fe/H] $= -2$. Most carbon stars (asterisks) are not plotted as they stretch beyond the plot limits along a line from the plotted ones up to $(V-K, U-B) \approx (6, 6)$.

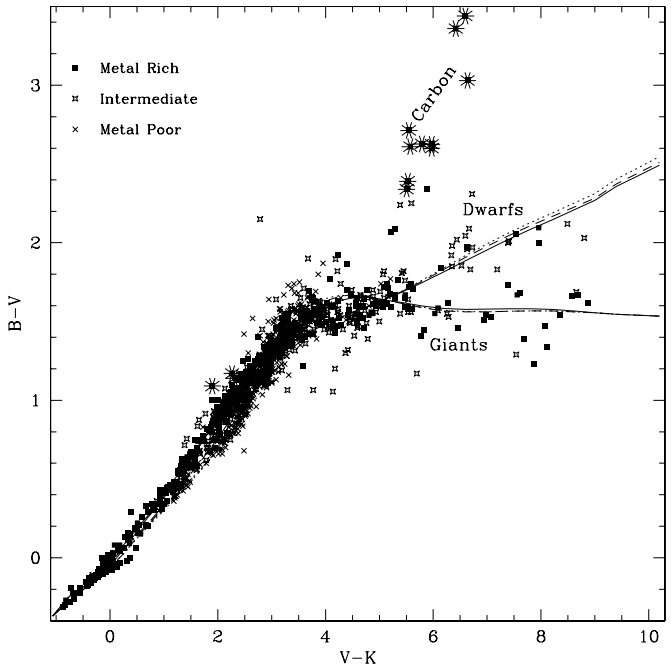

Figure 3. $B-V, V-K$ color–color diagram for unculled stars. Stars have different symbol types for metal-rich ([Fe/H] > -0.2), metal-poor ([Fe/H] < -1.2), and intermediate abundance ranges. Calibrations for typical giant and typical dwarf gravities are drawn in solid for [Fe/H] $= 0$, dashed for [Fe/H] $= -1$, and dotted for [Fe/H] $= -2$. Carbon stars are shown as asterisks.

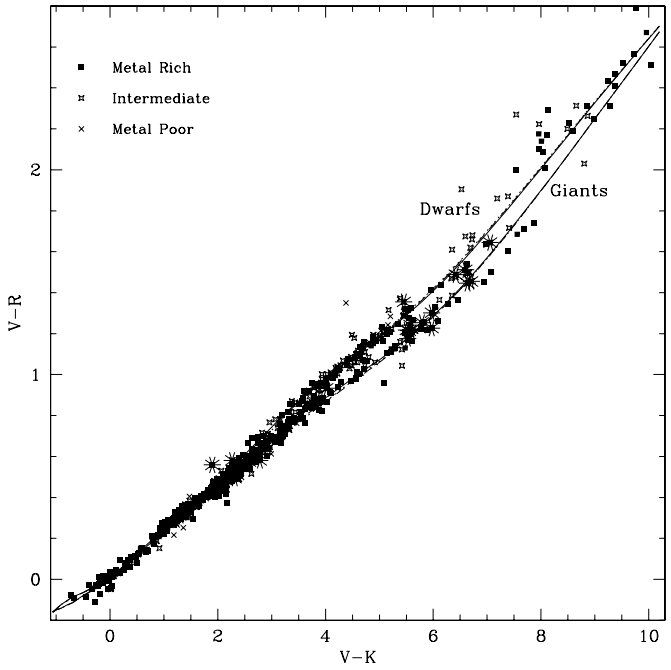

Figure 4. $V-R, V-K$ color–color diagram for unculled stars. Symbols and line styles are as in Figure 3.

did not influence the fits except for stars that do not exist in nature.

The final polynomials were combined in tabular form, using a weighted-mean scheme wherein the middle of each $V-K$ section was weighted strongly compared to the edges of each section. [Fe/H] and log g were tabulated in 0.5 dex intervals, $-2.5 \leqslant$ [Fe/H] $\leqslant 0.5$, and $-0.5 \leqslant \log g \leqslant 5.5$. The resultant color–color relations are illustrated in Figures 2, 3, 4, 5, 6, and 7. All stars, even if they were rejected during the fitting process, are included in the figures. Carbon stars are included, but only for illustrative purposes; fits were not attempted and one is again referred to the work of Bergeat et al. (2001).

For very hot stars of O and B spectral type an additional color–color table that was crafted by hand from either summary color-spectral type relations or from our own color–color relations was employed to refine the color–color relations for the hottest stars. The sources consulted were Schmidt-Kaler (1982), Tokunaga (2000), Vacca et al. (1996), and our own color–color plots. There is basically no abundance leverage for very hot stars, so we assumed a zero metallicity dependence. These tabulated average values were included in the polynomial fits as if they were individual stars.

In the hot star regime, two uncertain areas came to light that deserve mention as regards dwarf versus supergiant colors. First, in $U-B$, Schmidt-Kaler (1982) data imply a large and distinct color separation between dwarfs and supergiants, but the (few) supergiants available in our list did not follow the literature trend. Nor were the polynomials flexible enough to track these changes, mostly because, for O stars, the difference in surface gravity is very minor (4.15 (dwarfs) versus 4.09 (supergiants) according to Vacca et al. 1996). In the end, we performed a weighted average between the polynomial fits and the tabulated values. There is probably considerable uncertainty left in the supergiant $U-B$ colors, perhaps several tenths of a magnitude. This is one area that could be vastly improved with more photometry, with the caveats that reddening is often a huge factor for these intrinsically bright, usually distant stars and the fact that fast rotation introduces an inclination angle dependence in the colors. Users wishing to avoid this entirely may want to feed our interpolation program artificially high gravities for stars hotter than about 9000 K. The second area of debate was that the tabulated $H-K$ colors of Tokunaga (2000) for O supergiants

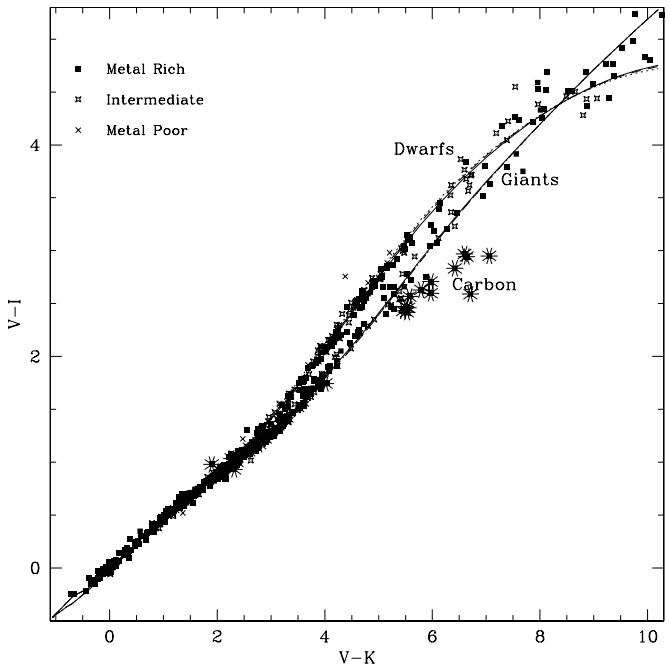

Figure 5. *V*−*I*, *V*−*K* color–color diagram for unculled stars. Symbols and line styles are as in Figure 3.

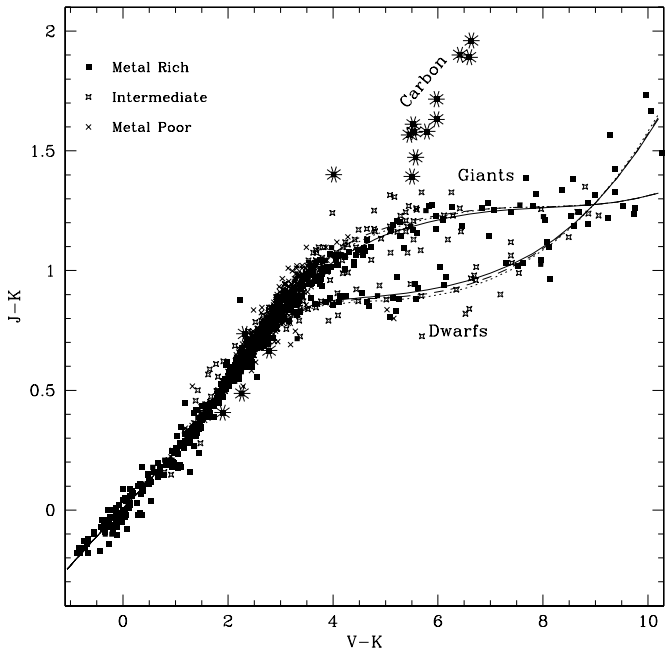

Figure 6. *J*−*K*, *V*−*K* color–color diagram for unculled stars. Symbols and line styles are as in Figure 3.

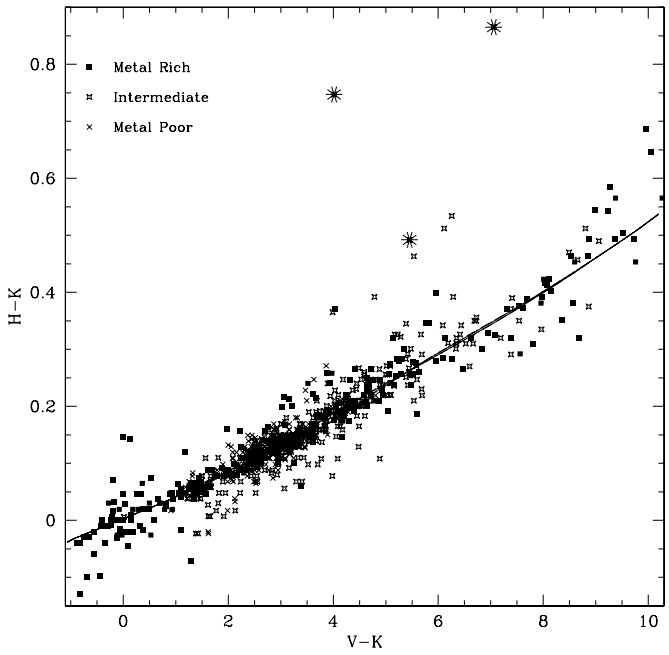

Figure 7. *H*−*K*, *V*−*K* color–color diagram for unculled stars. Symbols and line styles are as in Figure 3.

were about 0.09 mag redder than for O dwarfs. In this case, we saw no trace of such a trend in our data: a few stars were that red, but they were all dwarfs. We allowed the polynomial fit (which, in that regime, was a function of temperature alone) to determine the final color–color relation. In the middle of the temperature range, a small gravity dependence was indicated, but no dependence on [Fe/H] was ever statistically significant.

In the regime of cool giants, there is a strong evolutionary effect such that metal-poor stellar populations do not generate M-type giants. The rich globular cluster 47 Tucanae is on the cusp, containing four long-period variable stars at the tip of its giant branch at [Fe/H] ≈ -0.8. The SMC, at present-day [Fe/H] ≈ -0.6, generates some M and carbon stars, but mostly because of intermediate-age populations that grow very bright (and cool) asymptotic giant branches. Thus, there is a sharp transition from excellent metallicity coverage for K giants to very limited metallicity leverage for M giants, exacerbated by the fact that M giant abundances are hard to measure. In M dwarfs, where stars of all metallicities exist in our list, there is an interesting, strong convergence of color–color sequences as a function of metallicity so that G dwarfs have a very strong [M/H] dependence, there is a transition in K dwarfs, and M dwarf colors have no detectable [M/H] dependence. In fitting, therefore, the [M/H] dependence was gradually removed for cooler and cooler stars, for the giants because cool, metal-poor stars do not exist, and for the dwarfs because the [M/H] dependence removes itself empirically.

2.4. Temperatures

Due to our approach of fitting color–color relations internally as a function of gravity and abundance, attachment of temperature scales could, in principle, be done for any color–temperature relation in any part of the parameter space. The first iteration of this process was to layer color–temperature relations on top of each other until the whole parameter range was covered, and to take the median in regions where more than one relation applied. This is illustrated in Figures 8 and 9. For FGK giants Alonso et al. (1999a, 1999b) were used. These works include a specific [Fe/H] dependence, and the average of both *V*−*I* and *V*−*K* relations was used. For appropriate runs of temperatures and gravities, VandenBerg & Clem (2003) *V*−*I* was translated to *V*−*K* via our color–color relations. In a similar manner, the synthetic fluxes of R. L. Kurucz (1992, private communication) and Bessell et al. (1989, 1991) fluxes were combined and translated to colors as in Worthey (1994). In this case, both *V*−*R* and *V*−*I* were translated to *V*−*K* via the empirical color–color relations and plotted along with the untweaked (*V*−*K*)–$T_{\rm eff}$ relations. Tokunaga (2000) developed average color–temperature

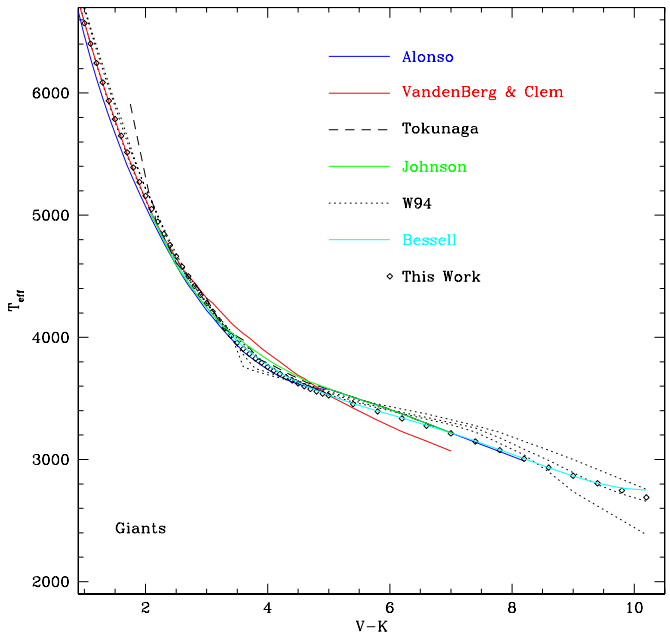

Figure 8. Temperature–($V-K$) calibrations for cool, solar abundance giants. Lines are color-coded for the calibrations of Alonso et al. (1999a, 1999b), VandenBerg & Clem (2003), Tokunaga (2000), Johnson (1966), Worthey (1994), and Bessell et al. (1998). Our adopted relation is shown as diamonds.

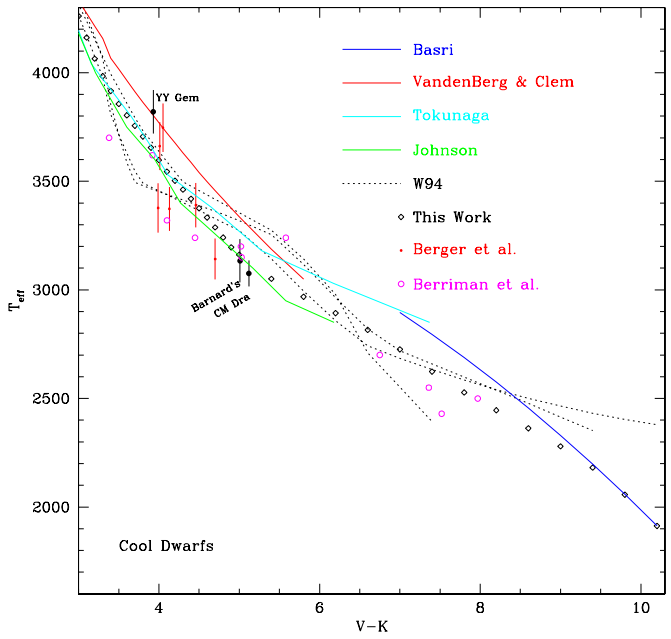

Figure 9. Temperature–($V-K$) calibrations for cool, solar abundance dwarfs. Lines are color-coded for the calibrations of VandenBerg & Clem (2003), Tokunaga (2000), Johnson (1966), Worthey (1994), Bessell et al. (1998), and Basri et al. (2000). Red dots with error bars are M dwarfs are from Berger et al. (2006) and magenta open circles are TIRFM temperatures and photometry from Berriman et al. (1992). YY Geminorum's temperature is from Torres & Ribas (2002), Barnard's star from Dawson & de Robertis (2004), and CM Draconis's from Viti et al. (1997). Our adopted relation is shown as diamonds.

relations for sequences of supergiants, giants, and dwarfs using literature temperature scales. Bessell et al. (1998) give color–temperature sequences for solar-abundance dwarfs and giants based on different model atmospheres, and we also referred to the empirical cool giant sequences of Ridgway et al. (1980) and Dyck et al. (1996). The color–temperature sequences of Johnson (1966) are also included. For the coolest dwarfs, analysis of the data of Basri et al. (2000) yielded a relation as a function of $I-K$ color, specifically $T_{\rm eff} = -460.25 \times (I-K) + 4323$, valid for $I - K > 2.9$. Adopting this relation meant that the final temperature assignments for the coolest dwarfs needed to wait for the final color relations to be fixed. Given the disparate ingredients, the final adopted temperatures were hand-guided a fair amount.

For example, M dwarfs with known angular diameters, but not separately summarized in existing color–$T_{\rm eff}$ calibrations, were also included in the mix. Eclipsing binaries YY Geminorum (Torres & Ribas 2002) and CM Draconis (Viti et al. 1997) were supplemented with interferometrically derived temperatures from Berger et al. (2006) and, in the case of Barnard's star, from Dawson & de Robertis (2004). *VK* photometry came from either our own catalog or that of Leggett et al. (2001). The temperature estimates of Berriman et al. (1992) for 11 dwarfs are also plotted. These are more indirect temperature estimates from the ratio of the bolometric flux to the flux at an infrared wavelength, the total to infrared flux ratio method (TIRFM). The position of especially the cooler stars was influential in our adopting a somewhat cooler temperature scale around 3000 K than the bulk of the published calibrations.

The fits are good to a limit of $V-K = 10.2$. Since cool dwarfs and giants have different temperature scales, this corresponds to approximately $T_{\rm eff} = 2700$ K for solar-metallicity giants and $T_{\rm eff} = 1914$ K for solar-metallicity dwarfs. Not that it proves or illustrates anything significant, but the Sun's $B-V$ comes out to be 0.66 mag in the final calibration, which compares well with literature estimates (Taylor 1994; Gray 1992, 1995).

2.5. Bolometric Corrections

The last item to be added was the V-band BC. Since they were that last item in the chain, BCs could be inserted as a function of color or of temperature and for any passband. As for temperature scales, a variety of empirical and theoretical options were intercompared. The VandenBerg & Clem (2003) BCs were adopted for the middle of the temperature range, supplemented by the Vacca et al. (1996) formula for $4.40 < \log T < 4.75$ for the hottest dwarfs and supergiants. VandenBerg & Clem (2003) have a solar $\mathrm{BC}_V = -0.09$ mag, and other scales were zero point adjusted to match. The Worthey et al. (1994) BCs needed a 0.03 mag shift to match that, for example. At the cool end, for both giants and dwarfs, the VandenBerg & Clem (2003) BCs drift slightly from most calibrations, as seen in Figure 10. For giants, we adopted the average, empirical-plus-theoretical K-band BC from Bessell et al. (1998), read from their Figure 20. For cool dwarfs, we adopt the K-band (UKIRT IRCAM3 system) BCs of Leggett et al. (2001). We extended their polynomial slightly to reach our $V - K = 10.2$ cool limit. One subtlety regarding the Leggett et al. (2001) calibration should be mentioned. They give two polynomial fits to the K-band BC, one as a function of $I-K$ and the other as a function of $J-K$. We adopt the $I-K$ version, as the $J-K$ version drifts significantly from the $I-K$ version at warmer temperatures. The cause of this drift is increased scatter in the $J-K$ diagram, or, more fundamentally, the fact that both J and K bands are on the red tail of the blackbody curve for the warm half of the temperature range covered, so that $J-K$ as a temperature indicator has a small temperature range per unit error.

The main calibrations employed are plotted in Figure 10, along with citations. For clarity, the fitted result and also the BCs of Buzzoni et al. (2010) are omitted. Note that, plotted as

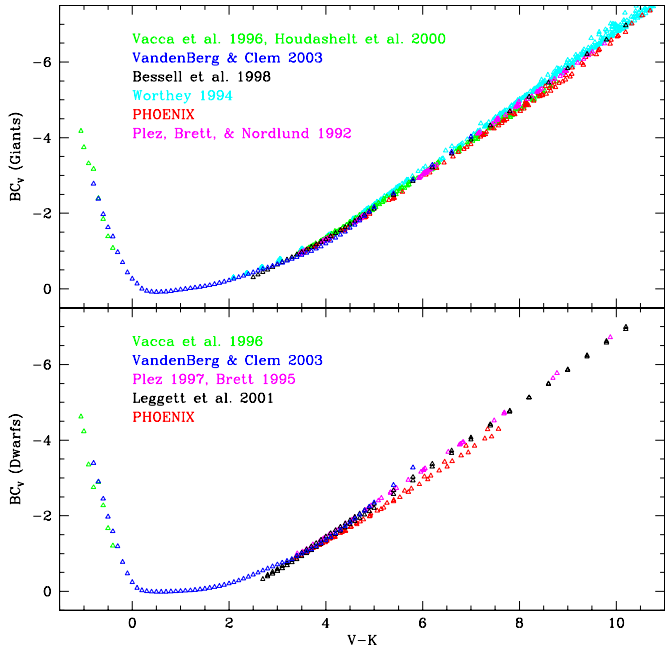

Figure 10. *V*-band bolometric corrections for dwarfs and giants. The top panel is a sequence of giants and the bottom panel is a sequence of dwarfs, both for near-solar metallicity. The symbol key is marked on the plot. The sources are Vacca et al. (1996) for hot stars, Houdashelt et al. (2000) for cool stars, VandenBerg & Clem (2003), Bessell et al. (1998), Worthey (1994), Plez et al. (1992), Brett (1995), and Leggett et al. (2001), plus "PHOENIX," which refers to fluxes produced from the Phoenix code (Allard & Hauschildt 1995) with colors generated as in Worthey (1994) and B. Plez (1997, private communication), subsequently published in Bessell et al. (1998).

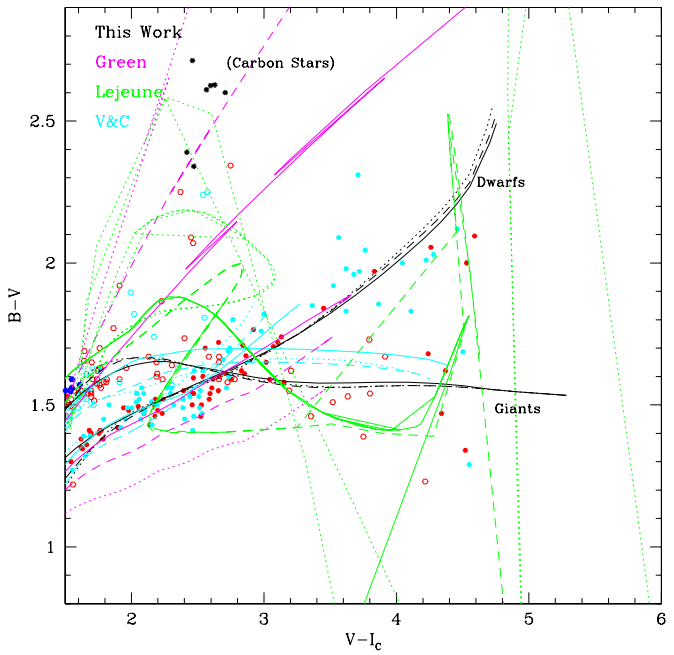

Figure 11. $B-V$, $V-I$ color–color diagram for M stars. Red dots are stars with [Fe/H] > -0.2 and blue dots are stars with [Fe/H] < -1.2 with intermediate stars indicated by cyan. Giants are open symbols, while dwarfs are filled. The data are unculled. Calibrations for giant and dwarf color–color sequences are drawn in solid for [Fe/H] $= 0$, dashed for [Fe/H] $= -1$, and dotted for [Fe/H] $= -2$. The color codes for different authors are noted in the figure ("Lejeune" is Lejeune et al. 1998, "Green" is the updated Green (1988) table, "V&C" is VandenBerg & Clem 2003).

a function of color, and as predicted by synthetic fluxes, the BCs are a very weak function of abundance and gravity. This is a degeneracy. That is, increasing a cool giant's abundance (for example) will make it redder and give it a larger (absolute value of the) *V*-band BC. Such vectors lie closely along the trend caused by temperature, so BCs are strongly covariant with T, log g, and [M/H] when plotted versus $V-K$. We exploit this for cool stars by adopting BCs that vary as a function of color alone. Gravity and abundance dependence then is inherited from the gravity and abundance variations of the color–color diagrams. The various relations were combined via temperature-dependent weighted means, where the weights were chosen to de-emphasize outliers.

3. COMPARISONS AND DISCUSSION

The wealth of comparison data that we could be checking against is too vast to illustrate completely in the pages of this journal, so we limit ourselves to a few key examples.

3.1. Cool Regime

One region of parameter space that is of keen interest is that of low stellar temperatures. We check our results for cool stars against VandenBerg & Clem (2003), Lejeune et al. (1998), an update of the Green (1988) color table used in the Yonsei–Yale isochrones (Yi et al. 2001), and, for good measure, the synthetic colors of Worthey (1994) in Figure 11. The coolest giants are very important for integrated-light studies of spectral features such as TiO that become strong only in these stars, and for surface brightness fluctuation (SBF) magnitudes, especially at red colors, that depend on these stars because of the L^2 dependence of an SBF magnitude.

In Figure 11, our fits are shown as black lines. They were fitted to the $(B-V)$–$(V-K)$ and $(V-I)$–$(V-K)$ diagrams, so it is no surprise that they still fit in this color–color plane. The updated Green calibration follows an extrapolation of the giant sequence off into regions not occupied by stars, while the dwarf sequence for solar abundance follows the stars very well. There is considerable metallicity dependence in the Green calibration that the stars do not appear to share. The VandenBerg & Clem (2003) sequences follow both dwarfs and giants fairly well, with a fairly good (small) abundance dependence. The oscillations in the solar-metallicity giant track are a reflection of actual values in their data tables. The coolest temperature reached by VandenBerg & Clem (2003) is 3000 K. The Lejeune et al. (1998) calibration is based on corrected synthetic fluxes. In this case, the dwarfs and giants track together with little or no gravity separation until, at a temperature well within the tabulated range of applicability, the values become wild.

3.2. Colors Not Explicitly Fit

Besides author comparisons, another way to check our results is to plot colors that were not fitted explicitly to see if the implicit color dependences are correctly modeled. $R-I$ is one such, and is illustrated in Figure 12. For this color, the fits were versus $V-R$ and $V-I$ for slightly different samples of stars. The $R-I$ fitted tracks fall among the stars fairly well, except for a hard-to-see reversal around $V-K = 1.5$ where the giants become $\approx$0.02 mag redder than the dwarfs. This 0.02 mag shift is probably incorrect, but it gives a valuable indication of the reliability of the color–color fits.

3.3. The K Dwarf Desert

Reliability must be a function of temperature regime. One particular troublesome area is that of K-type dwarfs and the

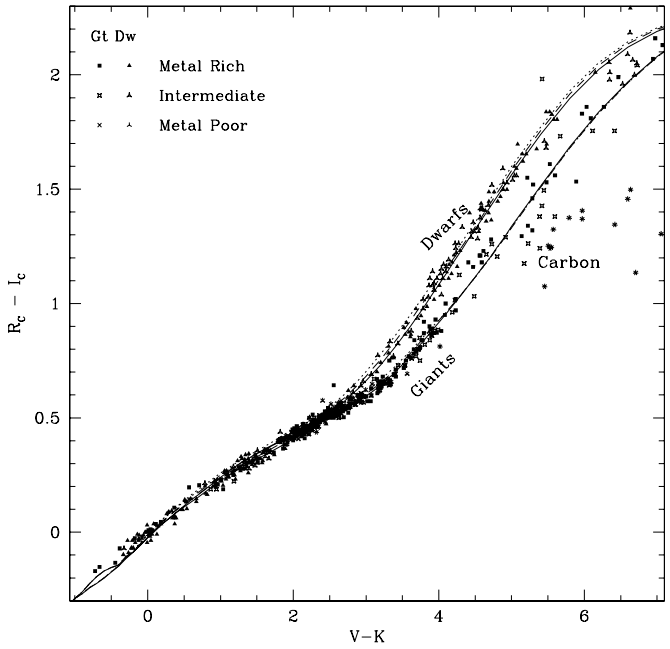

Figure 12. $R-I$ is plotted as a function of $V-K$. Stars of different giant/dwarf status and abundance are plotted with different symbols according to the key. Stars with [Fe/H] > -0.2 are considered metal-rich, stars with [Fe/H] < -1.2 are considered metal-poor, and stars between these values are considered intermediate in metallicity. Lines are coded as in Figure 11. This color was not fit during the calibration process.

Table 1
Median Polynomial Fit Uncertainty

Color	σ (mag)
$U-B$	0.071
$B-V$	0.017
$V-R$	0.010
$V-I$	0.011
$J-K$	0.004
$H-K$	0.002

damping of the abundance sensitivity going toward cool stars. In Figure 13, a $T_{\rm eff}$ of 5000 K corresponds to $V-K \approx 2.2$ and $T_{\rm eff} = 4000$ K corresponds to $V-K = 3.4$. It is clear that the magic combination of full photometry plus a good abundance estimate is lacking from our data set for dwarfs in general and metal-poor dwarfs in particular. Note the general lack of open symbols (dwarfs) compared to filled (giants). This lack of data means that the metallicity dependence of the dwarfs is inherited from the plentiful giants in this temperature regime, an undesirable feature. At redder colors, as their surface gravities diverge, the dwarfs and giants separate in color. Simultaneously, the metallicity dependence appears to reverse, at least in the giants. It is not completely clear from the present data what should be happening with the dwarfs, although they do seem to mirror the giants. The polynomials do their best to smoothly flow through all of this, but we judge it unlikely that they have truly captured the essence of the color behavior in this regime, as it is not clear to our eyes exactly what should be happening (it seems likely that some of the photometry is bad). The color reversal with [Fe/H] is an issue only for $U-B$ and $B-V$ colors, although the paucity of K dwarf data is of some concern for all colors, as the metallicity dependence is relatively unconstrained.

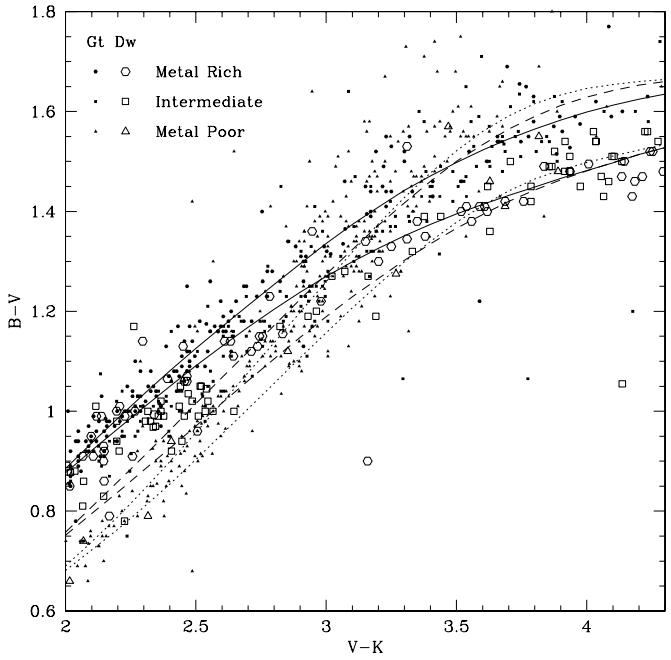

Figure 13. Small section of the $B-V$, $V-K$ color–color diagram. Dwarfs are drawn with larger symbols than giants for emphasis according to the key in the figure. Stars with [Fe/H] > -0.2 are considered metal-rich, stars with [Fe/H] < -1.2 are considered metal-poor, and stars between these values are considered intermediate in metallicity. Calibrations for giant and dwarf color–color sequences are drawn in solid for [Fe/H] $= 0$, dashed for [Fe/H] $= -1$, and dotted for [Fe/H] $= -2$. At red color, the dwarfs follow the bluer $B-V$ tracks. This is a region of uncertainty, as discussed in the text.

3.4. Error Propagation

The principal source of error in the color–color fits is finding a suitable polynomial to follow the various twists and turns that the colors take. We fit the colors in five segments, with multiply redundant overlap in color, and used the overlap regions to estimate the error from polynomial fitting. With typically hundreds of stars available for each fit, random photometric uncertainty is not a concern (though, of course, systematic uncertainty is). The median fit uncertainty over all temperatures, gravities, and abundances is listed in Table 1. We also thought it useful to propagate errors in the final subroutine so that uncertainties in the effective temperature scale could be translated to uncertainties in color. For this we used the various $T_{\rm eff}$ relations plotted in Figures 8 and 9 and a couple of others to roughly estimate a percentage error as a function of temperature. This is given in Table 2. Note that the errors in Table 2 for cool stars are more applicable to giants than dwarfs; dwarf temperatures seem more uncertain than those of giants, but we did not have enough dwarf calibrations to estimate this very well, so we left it alone. For color I with color error σ_I and a temperature error σ_T, errors propagate in the elementary way:

$$\sigma^2 = \sigma_I^2 + \left(\frac{dI}{dT}\sigma_T\right)^2. \quad (1)$$

3.5. Reddening Estimation Using M Dwarfs

Color–color diagrams have been used to derive a "color excess" from which can be inferred a value for the dust extinction (Morgan et al. 1953). The metallicity-dependent color–color fits of this paper offer a general, if not overly precise, method of generating a color–color plot for any color combination as

Table 2
Temperature Uncertainty Assumed

$T_{\rm eff}$ (K)	σ (%)
50000	4.0
20000	2.5
10000	1.0
6000	0.5
4000	0.5
3500	1.0
3000	1.5
2000	4.0

a function of abundance and gravity. The classic $U-B$, $B-V$ diagram is shown in Figure 14 for dwarfs only. The double inflection redward of zero color represents the rise and fall of the Balmer break in B-type through A- and F-type stars. A defect of this method is that it only works on clusters that have A-type stars, that is, the ones younger than about 1 Gyr that still have dwarfs that hot. Interestingly, there is an additional color inflection in the M dwarfs (cf. Lejeune et al. 1998), roughly between 4000 K and 3000 K, that may allow independent reddening estimates for old clusters that have deep photometry. This inflection exists in almost every color, although the U band presents the most dramatic manifestation of it.

The wiggle has been seen before in various colors and with variable fidelity (Caldwell et al. 1993; Bessell 1991; Tapia et al. 1988; Bryja et al. 1994) but with modern telescopes and instrumentation, it may turn into an astrophysical tool. It is caused by the onset of molecular absorption (TiO being the number one culprit) across the M temperature range that radically changes the underlying spectra shape (c.f. Bessell 1991).

If the U band is utilized, the coolest stars involved have $U - I = 5.65$ mag according to our colors and $M_I = 9.0$ according to diagrams in Leggett (1992). This leads to an absolute $M_U = 14.65$ mag. If a modest telescope can reach $U = 23$ as the KPNO 2.1 m did in Kaluzny & Rucinski (1995), then the U flux is readily detectable to about 500 pc distance. For reference, the nearest ancient open cluster is M67 at about 800 pc, so one would need a slightly larger telescope or better U sensitivity for U to be useful. However, redder colors can also be made to work at about the same confidence level relative to the fitting errors. The fitting errors are shown as error bars on points in Figure 14, as is another color sequence shifted by

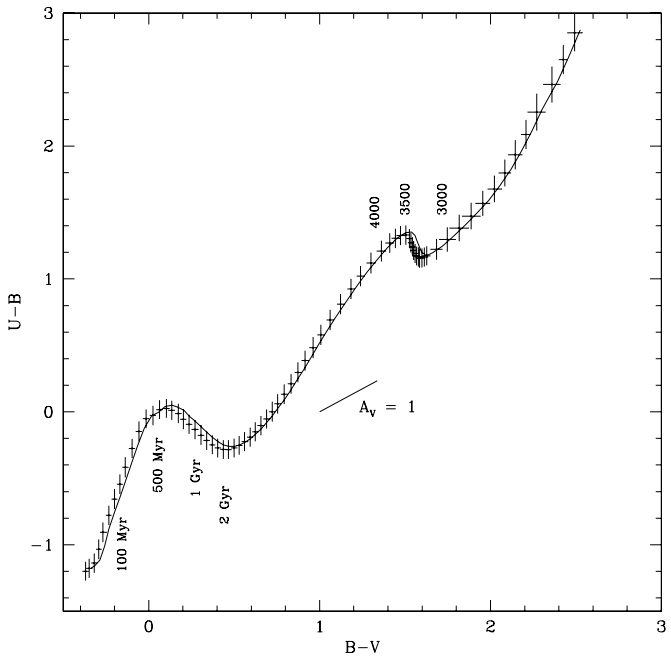

Figure 14. Final color–color calibration for dwarfs only is shown in the $U-B$, $B-V$ plane as dots with error bars attached, where the error bars include fitting uncertainties and $T_{\rm eff}$ uncertainties. An additional line is shown that represents the color shift due to dust screening of $A_V = 0.1$ mag. For illustrative purposes, a vector for $A_V = 1.0$ mag is also sketched. The approximate blue limits of the bluest dwarfs at the main-sequence turnoffs of isochrones of various ages are marked with the corresponding ages. Near the red bump feature, stellar effective temperatures (degrees K) are indicated.

$A_V = 0.1$, shown as a line. We judge that this extinction is the smallest that can be detected at all simply using the color–color fits we present, and so is not particularly competitive with other methods as it stands. Interestingly, at redder passbands, the M-type deflection becomes less pronounced but the errors also decrease so that any A_λ extinction vector stays at about the same statistical significance in most color–color planes. This does not solve the problem, however, because observational measurement error becomes larger than the fit error at *JHK* wavelengths. Future refinements to this reddening estimation method are possible and should be encouraged.

Giants also show such an inflection. However, no Galactic cluster has enough cool giants to populate the inflection region, globular cluster giant branches being too warm, and open

Table 3
Colors and Bolometric Correction Summary Table

$V-K$	$U-B$	$B-V$	$V-R$	$V-I$	$J-K$	$H-K$	$T_{\rm eff}$	BC$_V$
[Fe/H] = −2.5 and log g = −0.5								
−1.06	−1.200	−0.370	−0.160	−0.470	−0.251	−0.041	44000	−4.46
−1.00	−1.175	−0.344	−0.145	−0.435	−0.237	−0.038	38450	−4.03
−0.90	−1.141	−0.303	−0.122	−0.384	−0.213	−0.034	34174	−3.67
−0.80	−1.110	−0.262	−0.106	−0.329	−0.190	−0.030	30767	−3.32
−0.70	−1.068	−0.224	−0.083	−0.275	−0.166	−0.026	26892	−2.81
−0.60	−1.004	−0.200	−0.075	−0.244	−0.143	−0.022	23638	−2.31
−0.50	−0.947	−0.182	−0.066	−0.219	−0.119	−0.019	21296	−1.95
−0.40	−0.896	−0.167	−0.055	−0.196	−0.096	−0.015	18901	−1.67
−0.30	−0.796	−0.134	−0.048	−0.152	−0.073	−0.012	16645	−1.39
−0.20	−0.708	−0.109	−0.039	−0.117	−0.050	−0.008	14826	−1.09

(This table is available in its entirety in a machine-readable form in the online journal. A portion is shown here for guidance regarding its form and content.)

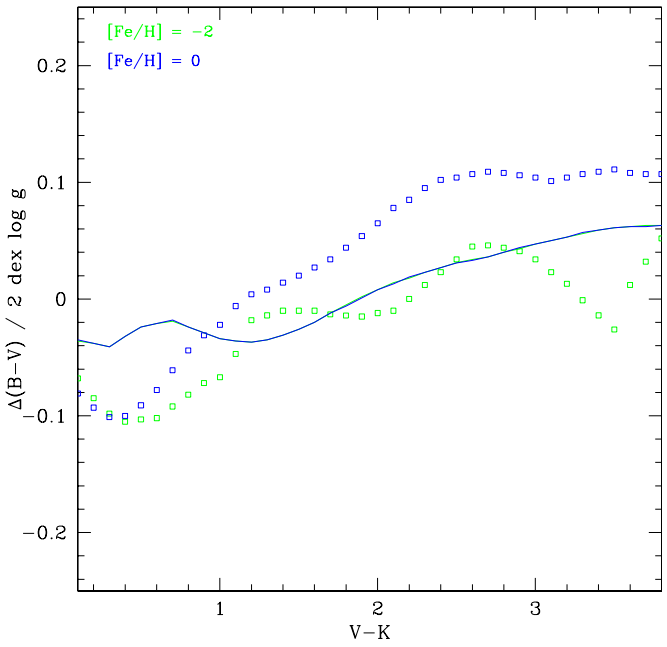

Figure 15. Change in $B-V$ color caused by a shift in log g from 2 to 4, plotted against $V-K$ color. Green lines or symbols indicate [Fe/H] $= -2$ and blue lines or symbols indicate [Fe/H] $= 0$. Lines are the present work, and both colors are present, but the lines coincide because there was no crosstalk between [Fe/H] and log g in the color–color fitting process. Symbols are Worthey (1994).

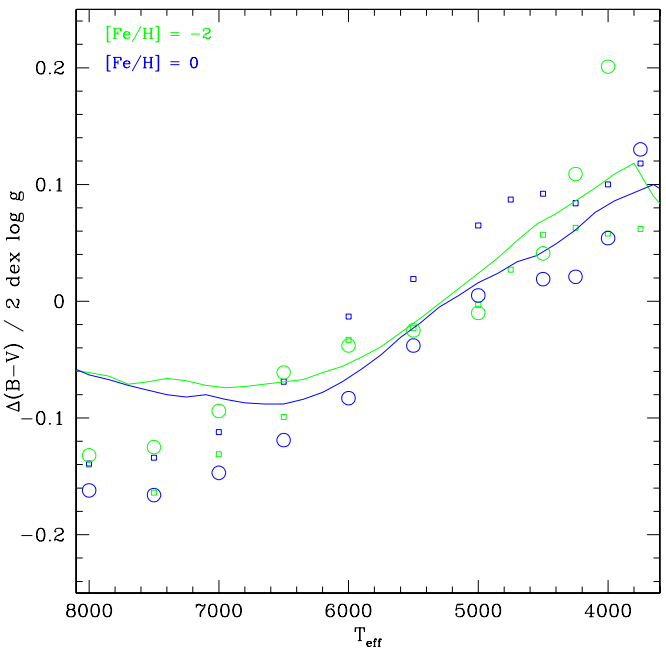

Figure 16. Change in $B-V$ color caused by a shift in log g from 2 to 4, plotted against $T_{\rm eff}$. Green lines or symbols indicate [Fe/H] $= -2$ and blue lines or symbols indicate [Fe/H] $= 0$. Lines are the present work, small symbols are Worthey (1994), and large symbols are the updated Green (1988) table.

clusters being too low-mass to have many such giants. There may be limited application for local group galaxy fields with resolved photometry; derivation of reddening maps across the surface, for example. However, the compositeness of the stellar populations of local galaxies may introduce too much error in the scheme for it to be useful.

3.6. Gravity Dependence Comparison

The dimension of temperature is a downstream add-on component using the method of this paper, but the dimensions of [Fe/H] and log g are inherited from the stellar catalog and can therefore be compared to the predictions from previous calibrations in a fairly clean way. In and near the M star temperature regime, we explicitly damped the [Fe/H] dependence away, but the gravity dependence was freely fit. The character of the data changes in that the dwarfs fork away from the giants the cooler one goes, making any dependence more complicated than linear rather suspicious. (No gravity dependence more than linear was used in this work, in this regime.) By way of illustration, we plot some color derivatives for one color, $B-V$, with abundance held fixed and gravity varied, in Figures 15 and 16.

Figures 15 and 16 show the same thing, except for the X-axis choice. The $V-K$ color (Figure 15) was what was fit against, and only calibrations that include both $B-V$ and $V-K$ can be included. Figure 16 is plotted against $T_{\rm eff}$ and can be compared to more calibrations. In the latter figure, also, the temperature scale difference causes the empirical trends to split.

The conclusions from examining these and similar figures for many colors are that the present work (1) resembles in gross other calibrations, (2) tends show the smallest, mildest gravity dependence, and (3) shows similar gravity dependence even at vastly different metallicity regimes. All three of these conclusions appear to be fairly robust, which should be a rather large concern, since the delta colors are quite substantial for most calibrations. An alarming example of this, not illustrated, is $U-B$ for stars hotter than the Sun, for which the empirical (this work) gravity dependence is essentially zero, but most other calibrations put it at $\Delta(B-V)/\Delta(\log g) \approx 0.15$ mag dex^{-1}.

3.7. Future Temperature Scale Adjustments

A topic beyond the scope of this paper deserves a comment, and that is attachment of this calibration to existing theoretical stellar evolutionary isochrones for purposes of comparing to star clusters and for purposes of integrated light studies. As a test case, which we intend to publish, multi-band photometry for two open clusters, M67 and NGC 6791, were collected from many sources and assembled into a *UBV RI JHK* data set. The color–color relations from these data sets agree well within expected errors with the color–color fits presented here.

However, the color–magnitude diagrams generated from Yi et al. (2001) isochrones and this work, when compared to the real clusters, are not so rosy. Figure 17 shows a color–magnitude diagram for open cluster M67, along with ellipses that represent 1σ errors on our color calibration, and there are drifts between isochrone and data that are substantially more than 1σ. Parenthetically, and with an emphatic lack of surprise, one of the places of mismatch is the late K dwarf region, among the temperatures where the empirical calibrations are competing with the VandenBerg & Clem (2003) semiempirical calibration. In that particular case, it is almost certainly the attachment of the temperatures in our calibration that is causing the wonkiness in the fit to the data.

In addition, for the finite set of data and models tried so far, a fit is often satisfactorily only in one color. When $B-V$ and V is fit, for example, $V-K$ and K do not fit for the same age and reddening. Going into the realm of theoretical stellar models introduces another layer of complexity that we are unable to cope with in this paper, but it seems clear that the temperature scale attached to our color–color relations is not, initially, going to mesh easily with existing isochrone sets. We conjecture that the blame will be shared between the temperature scale attached

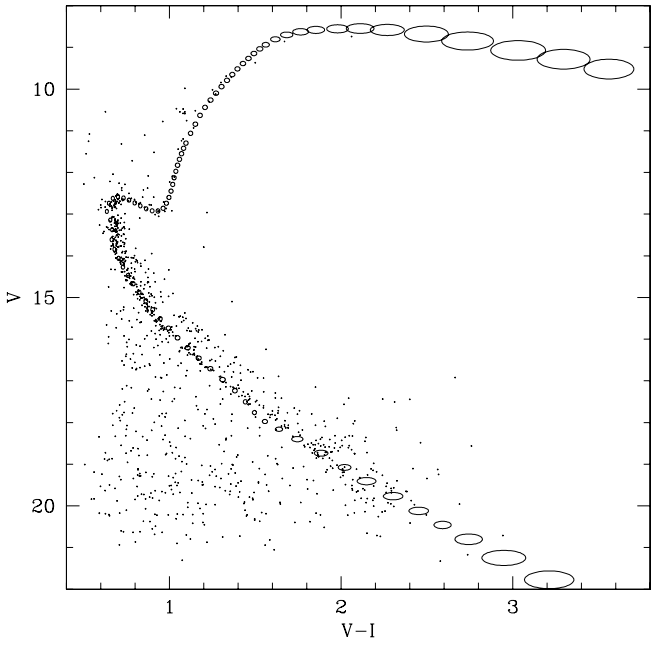

Figure 17. Color–magnitude diagram and isochrones for open cluster M67. The Yi et al. (2001) isochrones at solar metallicity and age 5 Gyr with the present color calibration is shown as ellipses that represent the propagated uncertainties. Distance modulus $(m-M)_V = 9.4$ and reddening $E(V-I) = 0.02$ are assumed. The data are that of Montgomery et al. (1993).

in this work, and the temperature scales established in theory via mixing length theory or other convection prescriptions.

4. SUMMARY AND CONCLUSION

Johnson/Cousins photometry was combined with literature [Fe/H] estimates to fit color–color diagrams as a function of gravity and abundance. Literature-average temperature and BC scales are attached to provide a global color–temperature relation for stars with $-1.06 < V - K < 10.2$. The *RI* magnitudes are in the Cousins system, and *JHK* magnitudes are in the Bessell homogenized system. Table 3, the full-length version of which is given in the online version of this journal, gives the final calibration in grid form. An ASCII version, interpolation program, and other supporting material are available at http://astro.wsu.edu/models/.

Several areas of improvement were noted in the main body of the paper, including filling photometry gaps, obtaining more accurate and on-system photometry, knowing better log g and [Fe/H] values, improving the statistics for data-impoverished groups of stars such as K dwarfs, applying small tweaks in the processing pipeline, and obtaining better empirical temperature and BC relations, especially for supergiants and M stars.

A way to estimate dust extinction from M dwarf colors arises from an inflection that exists in most colors relative to $V-K$. Unlike the classic *UBV* method, it can be used in old star clusters, but it does not seem to promise much, if any, increase in accuracy for clusters where both methods apply. The most sensitive band relative to photometric error for the new extinction measure is the *U* band, but if the *U* band is employed then clusters must be within a few hundred parsecs for ground-based observatories to able to measure adequate *U* fluxes.

Major funding was provided by the National Science Foundation grants AST-0307487, the New Standard Stellar Population Models project, and AST-0346347. The SIMBAD data base, NASA's Astronomical Data Center, and NASA's Astrophysics Data System were indispensable for this project. G.W. thanks the undergraduates who have typed in data pertaining to stars over more than 14 years this project has stretched: Brent Fisher (Worthey & Fisher 1996) and Joey Wroten at the University of Michigan and Jared Lohr and Ben Norman at Washington State University.

REFERENCES

Allard, F., & Hauschildt, P. H. 1995, ApJ, 445, 433
Alonso, A., Arribas, S., & Martinez-Roger, C. 1999a, A&AS, 139, 335
Alonso, A., Arribas, S., & Martinez-Roger, C. 1999b, A&AS, 140, 261
Basri, G., Mohanty, S., Allard, F., Hauschildt, P. H., Delfosse, X., Martín, E. L., Forveille, T., & Goldman, B. 2000, ApJ, 538, 363
Bell, R. A., & Gustafsson, B. 1989, MNRAS, 236, 653
Bergeat, J., Knapik, A., & Rutily, B. 2001, A&A, 369, 178
Berger, D. H., et al. 2006, ApJ, 644, 475
Berriman, G., Reid, N., & Leggett, S. K. 1992, ApJ, 392, L31
Bessell, M. S. 1979, PASP, 91, 589
Bessell, M. S. 1983, PASP, 95, 480
Bessell, M. S. 1991, AJ, 101, 662
Bessell, M. S., & Brett, J. M. 1988, PASP, 100, 1134
Bessell, M. S., Brett, J. M., Scholz, M., & Wood, P. R. 1991, A&AS, 89, 335
Bessell, M. S., Brett, J. M., Wood, P. R., & Scholz, M. 1989, A&AS, 77, 1 (erratum 87, 621 [1991])
Bessell, M. S., Castelli, F., & Plez, B. 1998, A&A, 333, 231 (erratum 337, 321)
Brett, J. M. 1995, A&A, 295, 736
Bryja, C., Humphreys, R. M., & Jones, T. J. 1994, AJ, 107, 246
Buser, R., & Kurucz, R. L. 1992, A&A, 264, 557
Buzzoni, A., Patelli, L., Bellazzini, M., Pecci, F. F., & Oliva, E. 2010, MNRAS, 403, 1592
Caldwell, J. A. R., Cousins, A. W. J., Ahlers, C. C., van Wamelen, P., & Maritz, E. J. 1993, South Afr. Astron. Obs. Circ., 15, 1
Cardelli, J. A., Clayton, G. C., & Mathis, J. S. 1989, ApJ, 345, 245
Carney, B. W. 1983, AJ, 88, 623
Carpenter, J. M. 2001, AJ, 121, 2851
Casagrande, L., Portinari, L., & Flynn, C. 2006, MNRAS, 373, 13
Cayrel de Strobel, G., Soubiran, C., & Ralite, N. 2001, A&A, 373, 159
Cohen, J. G., & Frogel, J. A. 1982, ApJ, 255, L39
Cohen, J. G., Frogel, J. A., & Persson, S. E. 1978, ApJ, 222, 165
Cohen, J. G., Frogel, J. A., Persson, S. E., & Zinn, R. 1980, ApJ, 239, 74
da Costa, G. S., & Armandroff, T. E. 1990, AJ, 100, 162
da Costa, G. S., Frogel, J. A., & Cohen, J. G. 1981, ApJ, 248, 612
Dahn, C. C., et al. 2002, AJ, 124, 1170
Dawson, P. C., & De Robertis, M. M. 2004, AJ, 127, 2909
Dyck, H. M., Benson, J. A., van Belle, G. T., & Ridgway, S. T. 1996, AJ, 111, 1705
Edvardsson, B., Andersen, J., Gustafsson, B., Lambert, D. L., Nissen, P. E., & Tomkin, J. 1993, A&A, 275, 101
Elias, J. H., Frogel, J. A., & Humphreys, R. M. 1985, ApJS, 57, 91
Elias, J. H., Frogel, J. A., Matthews, K., & Neugebauer, G. 1982, AJ, 87, 1029
Frogel, J. A., Mould, J., & Blanco, V. M. 1990, ApJ, 352, 96
Frogel, J. A., Persson, S. E., & Cohen, J. G. 1979, ApJ, 227, 499
Frogel, J. A., Persson, S. E., & Cohen, J. G. 1981, ApJ, 246, 842
Frogel, J. A., Persson, S. E., & Cohen, J. G. 1983, ApJS, 53, 713
Frogel, J. A., Persson, S. E., Matthews, K., & Aaronson, M. 1978, ApJ, 220, 75
Gray, D. F. 1992, PASP, 104, 1035
Gray, D. F. 1995, PASP, 107, 120
Gray, R. O., Corbally, C. J., Garrison, R. F., McFadden, M. T., Bubar, E. J., McGahee, C. E., O'Donoghue, A. A., & Knox, E. R. 2006, AJ, 132, 161
Gray, R. O., Corbally, C. J., Garrison, R. F., McFadden, M. T., & Robinson, P. E. 2003, AJ, 126, 2048
Green, E. M. 1988, in Calibration of Stellar Ages, ed. A. G. Davis Philip (Schenectady, NY: L. Davis), 81
Green, E. M., Demarque, P., & King, C. R. 1987, The Revised Yale Isochrones and Luminosity Functions (New Haven: Yale Observatory)
Houdashelt, M. L., Bell, R. A., Sweigart, A. V., & Wing, R. F. 2000, AJ, 119, 1424
Johnson, H. L. 1966, ARA&A, 4, 193
Kaluzny, J., & Rucinski, S. M. 1995, A&AS, 114, 1
Kurucz, R. L. 1992, RevMexAA, 23, 187
Leggett, S. K. 1992, ApJS, 82, 351
Leggett, S. K., Allard, F., Geballe, T. R., Hauschildt, P. H., & Schweitzer, A. 2001, ApJ, 548, 908

Lejeune, T., Cuisiner, F., & Buser, R. 1998, A&AS, 130, 65
McWilliam, A. 1990, ApJS, 74, 1075
Montgomery, K. A., Marschall, L. A., & Janes, K. A. 1993, AJ, 106, 181
Morel, M., & Magnenat, P. 1978, A&AS, 34, 477
Morgan, W. W., Harris, D. L., & Johnson, H. L. 1953, ApJ, 118, 92
Persson, S. E., Frogel, J. A., Cohen, J. G., Aaronson, M., & Mathews, K. 1980, ApJ, 235, 452
Plez, B., Brett, J. M., & Nordlund, A. 1992, A&A, 256, 551
Ridgway, S. T., Joyce, R. R., White, N. M., & Wing, R. F. 1980, ApJ, 235, 126
Schmidt-Kaler, T. 1982, in Landolt-Börnstein: Numerical Data and Functional Relationships in Science and Technology—New Series, Group 6, Astronomy and Astrophysics, Volume 2, Schaifers/Voigt: Astronomy and Astrophysics: Stars and Star Clusters, ed. L. H. Aller, I. Appenzeller, & B. Baschek (Berlin: Springer), 14
Stetson, P. B. 1981, AJ, 86, 687
Tapia, M., Roth, M., Marraco, H., & Ruiz, M.-T. 1988, MNRAS, 232, 661
Taylor, B. J. 1994, PASP, 106, 444
Tokunaga, A. T. 2000, in Astrophysical Quantities, ed. A. N. Cox (4th ed.; New York: Springer-Verlag), 143
Torres, G., & Ribas, I. 2002, ApJ, 567, 1140
Vacca, W. D., Garmany, C. D., & Shull, M. 1996, ApJ, 460, 914
VandenBerg, D. A., & Clem, J. L. 2003, AJ, 126, 778
Vazdekis, A., Casuso, E., Peletier, R. F., & Beckman, J. E. 1996, ApJS, 106, 307
Veeder, G. J. 1974, AJ, 79, 1056
Viti, S., Jones, H. R. A., Schweitzer, A., Allard, F., Hauschildt, P. H., Tennyson, J., Miller, S., & Longmore, A. J. 1997, MNRAS, 291, 780
von Braun, K., Chiboucas, K., Minske, J. K., Salgado, J. F., & Worthey, G. 1998, PASP, 110, 810
Wood, P. R., & Bessell, M. S. 1983, ApJ, 265, 748
Wood, P. R., Bessell, M. S., & Fox, M. W. 1983, ApJ, 272, 99
Worthey, G. 1994, ApJS, 95, 107
Worthey, G., Faber, S. M., González, J. J., & Burstein, D. 1994, ApJS, 94, 687
Worthey, G., & Fisher, B. 1996, BAAS, 189, 72.05
Worthey, G., & Jowett, K. J. 2003, PASP, 115, 96
Yi, S., Demarque, P., Kim, Y.-C., Lee, Y.-W., Ree, C. H., Lejeune, T., & Barnes, S. 2001, ApJS, 136, 417